Topological Representations of Vector Fields

Holger Theisel[1], Christian Rössl[2], and Tino Weinkauf[3]

[1] Bielefeld University theisel@techfak.uni-bielefeld.de
[2] INRIA Sophia-Antipolis christian.roessl@sophia.inria.fr
[3] Zuse Institute Berlin (ZIB) weinkauf@zib.de

Summary. This chapter gives an overview on topological methods for vector field processing. After introducing topological features for 2D and 3D vector fields, we discuss how to extract and use them as visualization tools for complex flow phenomena. We do so both for static and dynamic fields. Finally, we introduce further applications of topological methods for compressing, simplifying, comparing, and constructing vector fields.

1 Introduction

Vector fields appear in many areas of science, engineering, and industry. In recent years, a variety of methods to process, model, analyze and visualize vector fields have been developed. Similar to other areas of Computer Graphics, a common challenge is the dramatically increasing size and complexity of the vector fields. One common approach to processing vector fields is *feature extraction* [24]. Features represent certain interesting objects or structures in the vector field like topological features, vortex core lines, or shock waves. The idea of feature extraction is to detect, extract and track these features and use them instead of the whole data set for further processing.

Among the feature extraction techniques, topological methods have gained a rather high popularity because they offer to describe even complex flow behaviors by only a limited number of graphical primitives. The main idea of them is to segment the vector field into areas of different flow behavior.

Topological structures are well-studied in the context of dynamical systems and partial differential equations [1, 3, 10]. However, in recent years they attracted the Visualization community, leading to a quite intensive research on how to use them as visualization tools.

In this chapter, we give an overview of topological methods for vector field processing. The main class of applications we have in mind is the visualization of flow structures (sections 2–4). In addition, we discuss further applications of topological methods for vector fields (section 5).

2 Topological features of 2D vector fields

2.1 Concepts

To describe topological features of 2D vector fields in detail, we start with a steady 2D vector field

$$\mathbf{v}(x,y) = \begin{pmatrix} u(x,y) \\ v(x,y) \end{pmatrix} \tag{1}$$

and assume $\mathbf{v}$ to be continuous and differentiable. Then the *Jacobian matrix* $\mathbf{J_v}$ is a 2×2 matrix which is defined in every point of the domain of the vector field by

$$\mathbf{J_v}(x,y) = (\mathbf{v}_x, \mathbf{v}_y) = \begin{pmatrix} u_x(x,y) & u_y(x,y) \\ v_x(x,y) & v_y(x,y) \end{pmatrix}. \tag{2}$$

The determinant of $\mathbf{J_v}$ is called *Jacobian* of $\mathbf{v}$.

A point $\mathbf{x}_0 \in E_2$ is called a *critical point* if $\mathbf{v}(\mathbf{x}_0) = (0,0)^T = \mathbf{0}$ and $\mathbf{v}(\mathbf{x}) \neq \mathbf{0}$ for any $\mathbf{x} \neq \mathbf{x}_0$ in a certain neighborhood of $\mathbf{x}_0$.

A *stream line* $\mathbf{s}(t)$ of the vector field $\mathbf{v}$ is a curve in the domain of $\mathbf{v}$ with

$$\dot{\mathbf{s}}(t) = \mathbf{v}(\mathbf{s}(t)) \tag{3}$$

for any t of the domain of $\mathbf{s}$. In (3), $\dot{\mathbf{s}}$ denotes the tangent vector of $\mathbf{s}$. Considering the vector field $\mathbf{v}$ as the velocity field of a steady flow, a stream line describes the path of a massless particle set out at a certain location in the flow.

Stream lines do not intersect each other (except for critical points of $\mathbf{v}$). Given a point in the flow, there is one and only one stream line through it (except for critical points of $\mathbf{v}$).

Classification of critical points

To classify a critical point in a 2D steady vector field, sectors of different flow behavior around it have to be considered. Three kinds of sectors can be distinguished ([7]):

- In a *parabolic sector* either all stream lines end, or all stream lines originate, in the critical point. Figure 1a shows an example.
- In a *hyperbolic sector* all stream lines pass by the critical point, except for two stream lines being the boundaries of the sector. One of these two stream lines ends in the critical point while the other one originates in it. Figure 1b shows an example.
- In an *elliptic sector* all stream lines originate and end in the critical point. Figure 1c shows an example.

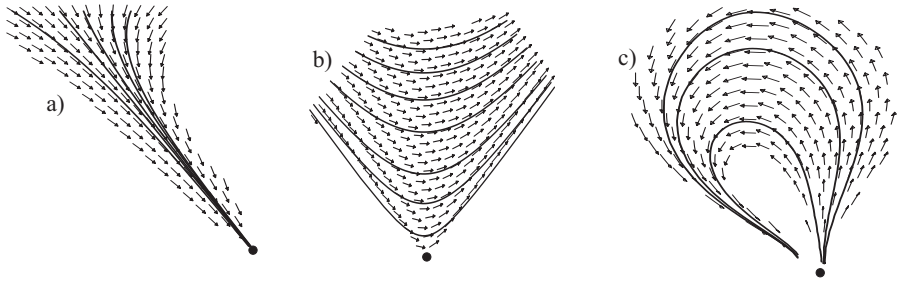

Fig. 1. Sectors of a critical point; a) parabolic sector; b) hyperbolic sector; c) elliptic sector (from [42]).

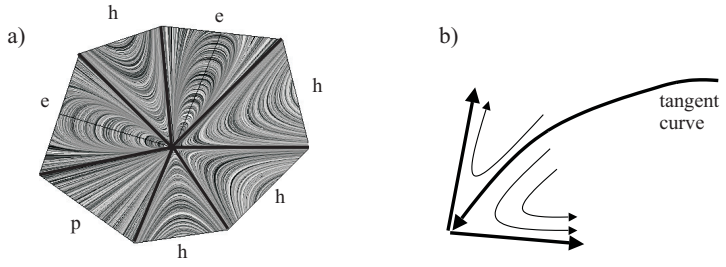

Fig. 2. a) general critical point; b) stream line separating two hyperbolic sectors.

A critical point in a 2D vector field is completely classified by specifying number and order of all sectors around it. Consider figure 2a for an example. This critical point consists of 7 sectors in the following order: hyperbolic, elliptic, hyperbolic, elliptic, parabolic, hyperbolic, hyperbolic.

The different sectors are delimited by stream lines originating or ending in the critical point. Figure 2b shows such a stream line delimiting two hyperbolic sectors.

Each critical point can be assigned an *index*:

$$\text{index} = 1 + \frac{n_e - n_h}{2} \tag{4}$$

where n_e is the number of elliptic sectors and n_h is the number of hyperbolic sectors. The index can also be interpreted as the number of counterclockwise revolutions made by the vectors of $\mathbf{v}$ while travelling counterclockwise on a closed curve around the critical point (the closed curve must be so tight to the critical point that no other critical point is inside it).

The index can be considered as an overview of the complexity of a critical point but does not cover the complete classification: there are critical points with different sectors but the same index. An further introduction to the classification of 2D critical points and their indices can be found in [7].

A critical point $\mathbf{x}_0$ in the vector field $\mathbf{v}$ is called a *first-order critical point* if the Jacobian does not vanish in $\mathbf{x}_0$; otherwise the critical point is called *high-order critical point*. As shown in [13] and [14], the classification of critical points $\mathbf{x}_0 = (x_0, y_0)$ in the vector field $\mathbf{v}$ simplifies if $\mathbf{x}_0$ is a first order critical point. In this case a first order Taylor expansion

$$\mathbf{v}_{T1,\mathbf{x}_0} = \begin{pmatrix} u_x(\mathbf{x}_0) & u_y(\mathbf{x}_0) \\ v_x(\mathbf{x}_0) & v_y(\mathbf{x}_0) \end{pmatrix} \cdot \begin{pmatrix} x - x_0 \\ y - y_0 \end{pmatrix} \tag{5}$$

of the flow around $\mathbf{x}_0$ is sufficient to obtain the complete classification of it. (5) ensures that

$$\mathbf{J}_\mathbf{v}(\mathbf{x}_0) = \mathbf{J}_{\mathbf{v}_{T1,\mathbf{x}_0}}(\mathbf{x}_0). \tag{6}$$

It turns out that for $\det(\mathbf{J}_\mathbf{v}(\mathbf{x}_0)) < 0$, the critical point $\mathbf{x}_0$ consists of 4 hyperbolic sectors and therefore has an index of -1. A critical point of this classification is called a *saddle point*. In this case the eigenvectors of $\mathbf{J}_\mathbf{v}(\mathbf{x}_0)$ denote the delimiters of the hyperbolic areas around $\mathbf{x}_0$. For $\det(\mathbf{J}_\mathbf{v}(\mathbf{x}_0)) > 0$, the critical point $\mathbf{x}_0$ consists of one parabolic sector and therefore has an index of $+1$.

This classification of a first order critical point $\mathbf{x}_0$ with an index of $+1$ can be refined by considering the eigenvalues of $\mathbf{J}_\mathbf{v}(\mathbf{x}_0)$. Let R_1, R_2 be the real parts of the eigenvalues of $\mathbf{J}_\mathbf{v}(\mathbf{x}_0)$, and let I_1, I_2 be the imaginary parts of the eigenvalues of $\mathbf{J}_\mathbf{v}(\mathbf{x}_0)$. Then the refined classification following [13] is shown in figure 3. Note that positive real parts denote a repelling behavior of the flow while negative real parts indicate an attracting behavior. Non-zero imaginary parts denote a circulating behavior of the flow. [23] detects and

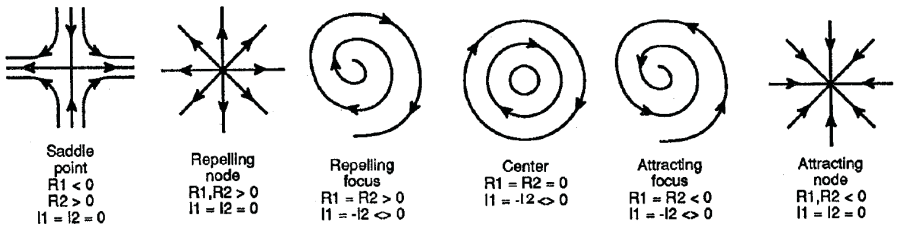

Fig. 3. Classification of first order critical points; R_1, R_2 denote the real parts of the eigenvalues of the Jacobian matrix while I_1, I_2 denotes its imaginary parts (from [13]).

classifies critical points using a discrete Hodge decomposition.

Boundary switch points

Vector fields are usually defined over a limited domain. Along its boundary curves, the vector field has either an inflow or an outflow behavior. *Boundary*

switch points separate these areas. A boundary switch point is a point on the boundary curve with the property that the tangent of the boundary curve is parallel to the vector of the field there. Two kinds of boundary switch points can be distinguished: inbound or outbound points. At an inbound point, the stream line starting there in forward and backward direction goes into the domain of **v**, while for an outbound point it leaves the domain immediately. Figure 4 (a) and (b) give an illustration.

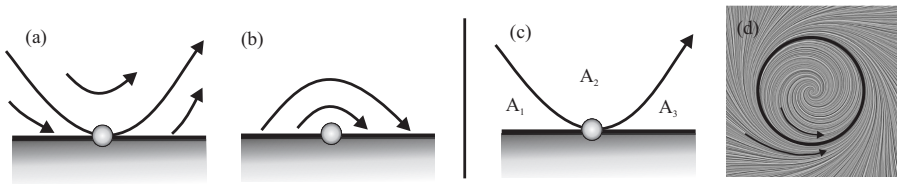

Fig. 4. (a) inbound boundary switch point; (b) outbound boundary switch point; (c) separatrix from inbound boundary switch points divides the domain into 3 sectors A_1, A_2, A_3; (d) an isolated closed stream line divides the domain into 2 sectors.

Separatrices

Separatrices are stream lines which divide the domain of **v** into areas of different flow behavior. Different types of separatrices are possible:

- Each tangent curve originating/ ending in the critical point and separating two sectors there is a separatrix. Figure 2b illustrates a separatrix which separates two hyperbolic sectors of a critical point.
- Stream lines from inbound boundary switch points divide the domain into 3 different areas. Figure 4(c) gives an illustration.
- Isolated closed stream lines are separatrices. Figure 4(d) gives an illustration.

2.2 Visualizing 2D topology

After the introduction of topological methods as a visualization tool for 2D vector fields in [13], an intensive research has been done in this field. [26] treats higher order critical points. In [5], separatrices starting from boundary switch points are discussed. [46] and [37] give methods to detect closed separatrices. To visualize the topology of a 2D vector field, critical points, boundary switch points, and separatrices have to be extracted. Critical points can be extracted directly (in case of a piecewise (bi-)linear vector field) or numerically. Also, boundary switch points can be found by a closed solution.

Most visualization approaches consider only first order critical points. Then the starting directions of the separatrices are the eigendirections of the Jacobian matrices at the saddle points.

For integrating stream lines (for instance separatrices), usually numerical methods are applied[4]. Standard is a fourth order Runge-Kutta integration [27]. Figure 5 shows an example of a topological skeleton of a 2D vector field

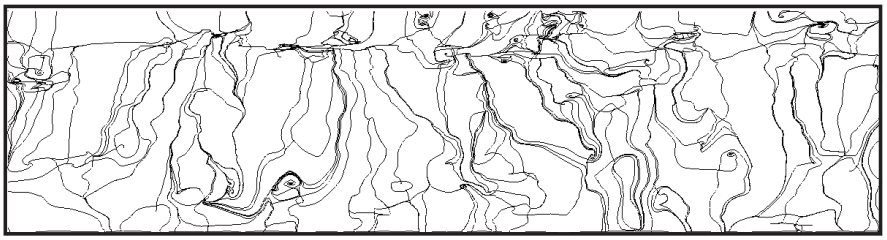

Fig. 5. Topological skeleton of the skin friction data set.

describing the skin friction on a face of a cylinder[5].

Isolated closed stream lines can only be extracted and visualized by a global analysis of the vector field. [46] uses the underlying grid structure of a piecewise linear vector field: each grid cell is analyzed concerning the re-entering behavior of the stream lines starting at its boundaries. [37] presents an approach which uses the fact that searching isolated stream lines in 2D vector fields corresponds to intersecting stream surfaces in certain 3D vector fields. Figure 6 gives an illustration.

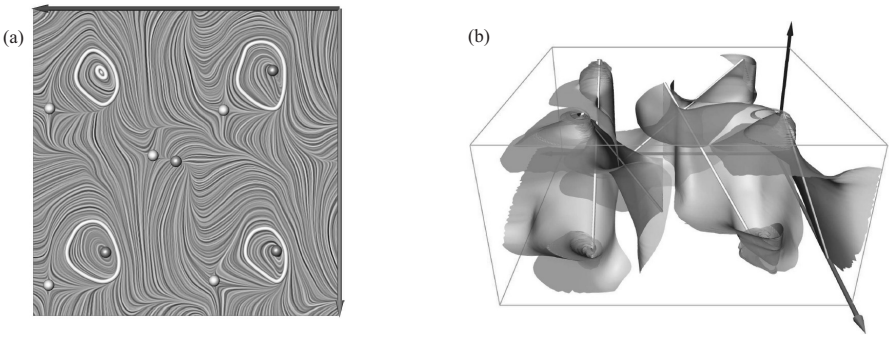

Fig. 6. (a) detected closed stream lines in a 2D vector field; (b) to get them, certain stream surfaces of a 3D vector field are integrated and intersected (from [37]).

[4] Only for piecewise linear vector fields, a closed solution exists [21].

[5] The data set was generated by R.W.C.P. Verstappen and A.E.P. Veldman of the University of Groningen (the Netherlands).

3 Topological Features of 3D Vector Fields

3.1 Concepts

Topological structures of 3D vector fields are well-understood in the visualization community for many years [14, 2, 4, 22]. In this section, we collect the most important concepts and properties.

Critical points

Given a 3D vector field $\mathbf{v} : \mathbb{E}^3 \rightarrow \mathbb{R}^3$, a first order critical point $\mathbf{x}_0$ (i.e., a point $\mathbf{x}_0$ with $\mathbf{v}(\mathbf{x}_0) = \mathbf{0}$ and $\det(\mathbf{J}_\mathbf{v}(\mathbf{x}_0)) \neq 0$, where $\mathbf{J}_\mathbf{v}(\mathbf{x}) = \nabla\mathbf{v}(\mathbf{x})$ is the Jacobian matrix of $\mathbf{v}$, can be classified by an eigenvalue/eigenvector analysis of $\mathbf{J}_\mathbf{v}(\mathbf{x}_0)$. Let $\lambda_1, \lambda_2, \lambda_3$ be the eigenvalues of $\mathbf{J}_\mathbf{v}(\mathbf{x}_0)$ ordered according to their real parts, i.e. $Re(\lambda_1) \leq Re(\lambda_2) \leq Re(\lambda_3)$. Furthermore, let $\mathbf{e}_1, \mathbf{e}_2, \mathbf{e}_3$ be the corresponding eigenvectors, and let $\mathbf{f}_1, \mathbf{f}_2, \mathbf{f}_3$ be the eigenvectors of the transposed Jacobian $(\mathbf{J}_\mathbf{v}(\mathbf{x}_0))^T$ corresponding to $\lambda_1, \lambda_2, \lambda_3$. (Note that $\mathbf{J}$ and $\mathbf{J}^T$ have the same eigenvalues but not necessarily the same eigenvectors.) Concerning the real parts of the eigenvalues, the following classification of critical points is possible:

- sources: $0 < Re(\lambda_1) \leq Re(\lambda_2) \leq Re(\lambda_3)$
- repelling saddles: $Re(\lambda_1) < 0 < Re(\lambda_2) \leq Re(\lambda_3)$
- attracting saddles: $Re(\lambda_1) \leq Re(\lambda_2) < 0 < Re(\lambda_3)$
- sinks: $Re(\lambda_1) \leq Re(\lambda_2) \leq Re(\lambda_3) < 0$

Each of these classes can be further divided into two stable[6] subclasses by deciding if imaginary parts in the eigenvalues are present. Since vector fields usually consist of a finite number of critical points, an iconic representation is the appropriate visualization approach. Several icons have been proposed in the literature, see [14, 9, 19, 11]. In the following we describe the different classes of critical points as well as the icons which were used in [36, 43] for their visual representation. These icons were colored depending on the flow behavior: Attracting parts (inflow) are colored blue, while repelling parts (outflow) are colored red.

Sources and Sinks

A source $\mathbf{x}_{So}$ is characterized by the fact that in its neighborhood all stream lines diverge from $\mathbf{x}_{So}$. The two stable subclasses are repelling nodes and repelling foci.

A *repelling node* is characterized by the absence of imaginary parts in $\lambda_1, \lambda_2, \lambda_3$, and $\mathbf{e}_1, \mathbf{e}_2, \mathbf{e}_3$ are linearly independent (Figure 7a). To visualize a

[6] A critical point in $\mathbf{v}$ is called stable if a small perturbation of $\mathbf{v}$ does not change the classification of the critical point.

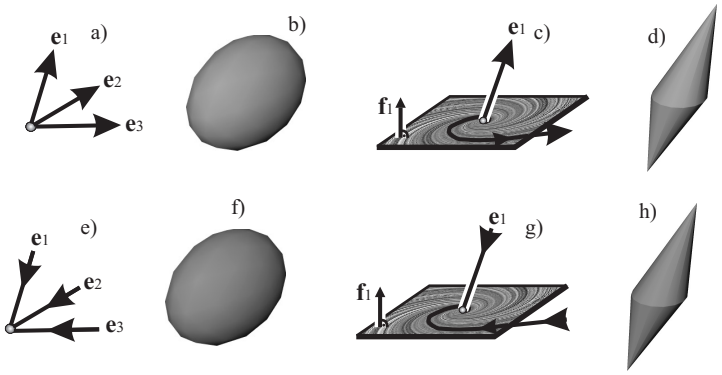

Fig. 7. Sources and sinks; (a) repelling node and (b) its icon; (c) repelling focus and (d) its icon; (e) attracting node and (f) its icon; (g) attracting focus and (h) its icon (from [43]).

repelling node, we use a red ellipsoid with a shape determined by the eigenvectors and eigenvalues of the Jacobian (Figure 7b).

A *repelling focus* is characterized by the presence of two eigenvalues with imaginary parts, say λ_2, λ_3. In this case, the only real eigenvector $\mathbf{e}_1$ of $\mathbf{J}$ describes the direction of straight outflow. In addition, there is a plane in which a 2D repelling focus behavior appears. This plane is perpendicular to the only real eigenvector $\mathbf{f}_1$ of $\mathbf{J}^T$ (Figure 7c). As an icon, we used a red double cone representing the outflow plane and the outflow direction by its shape (Figure 7d).

A sink $\mathbf{x}_{Si}$ can be considered as an inverse source: in its neighborhood all stream lines converge to $\mathbf{x}_{Si}$. The two subcases are *attracting nodes* (Figures 7e-f) and *attracting foci* (Figures 7g-h).

Repelling Saddles and Attracting Saddles

A repelling saddle $\mathbf{x}_R$ has one direction of inflow behavior (called *inflow direction*) and a plane in which a 2D outflow behavior occurs (called *outflow plane* through $\mathbf{x}_R$). For all other directions around $\mathbf{x}_R$, the stream lines do not touch $\mathbf{x}_R$. The two stable subclasses are repelling node saddles and repelling focus saddles.

A *repelling node saddle* has no imaginary parts in $\lambda_1, \lambda_2, \lambda_3$, and $\mathbf{e}_1, \mathbf{e}_2, \mathbf{e}_3$ are linearly independent (Figure 8a). Its icon includes a red ellipse denoting the outflow plane defined by $\mathbf{e}_2, \mathbf{e}_3$ and λ_2, λ_3, while a blue arrow pointing to the center of the ellipse represents the inflow direction (Figure 8b).

A *repelling focus saddle* is characterized by $Im(\lambda_2) = -Im(\lambda_3) \neq 0$. Here, the only real eigenvector $\mathbf{e}_1$ of $\mathbf{J}$ describes the inflow direction. The only real eigenvector $\mathbf{f}_1$ of $\mathbf{J}^T$ describes the plane with the 2D repelling focus behavior (Figures 8c-d).

An attracting saddle $\mathbf{x}_A$ can be interpreted as an inverse version of a repelling saddle. It has one direction of outflow behavior (*outflow direction*) and a plane in which a 2D inflow behavior appears (*inflow plane* through $\mathbf{x}_A$). The two stable subclasses are *attracting node saddles* without imaginary parts of the eigenvalues (Figures 8e-f) and *attracting focus saddles* (Figures 8g-h).

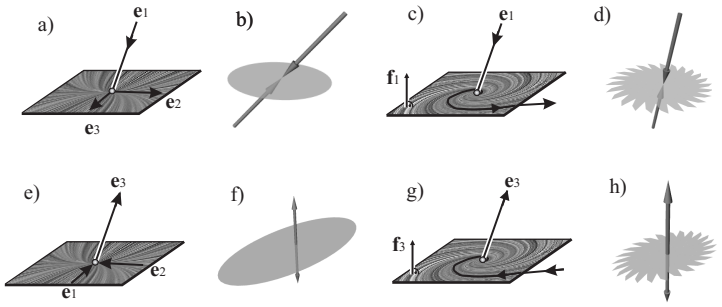

Fig. 8. Repelling and attracting saddles; (a) repelling node saddle and (b) its icon; (c) repelling focus saddle and (d) its icon; (e) attracting node saddle and (f) its icon; (g) attracting focus saddle and (h) its icon (from [43]).

Unstable Critical Points

In addition to the kinds of critical points described above, a number of unstable versions of sources, sinks and repelling/attracting saddles exist. Also, two further classes of unstable critical points exist which do not belong to any of the above-mentioned classes: attracting centers and repelling centers. A repelling center is characterized by $Re(\lambda_1) = Re(\lambda_2) = 0 < Re(\lambda_3)$ and $Im(\lambda_1) = -Im(\lambda_2) \neq 0$. It consists of one direction $\mathbf{e}_3$ of outflow behavior and one plane perpendicular to $\mathbf{f}_3$ with a 2D circulating behavior. An attracting center has $Re(\lambda_1) < 0 = Re(\lambda_2) = Re(\lambda_3)$ and $Im(\lambda_2) = -Im(\lambda_3) \neq 0$. The inflow direction is defined by $\mathbf{e}_1$ and the 2D circulating behavior can be found in the plane perpendicular to $\mathbf{f}_1$.

Boundary switch curves

Consider the 3D vector field $\mathbf{v}$ in the domain

$$D = (x_{min}, x_{max}) \times (y_{min}, y_{max}) \times (z_{min}, z_{max}) \tag{7}$$

with $x_{min} < x_{max}$, $y_{min} < y_{max}$, $z_{min} < z_{max}$. The boundary surfaces of D (which are the 6 faces of the bounding box) consist of outflow and inflow areas which are separated by *boundary switch curves*. Boundary switch curves consist of all points on the boundary where the flow direction is tangential to the boundary surface. Figure 9(a) illustrates an example of the boundary plane

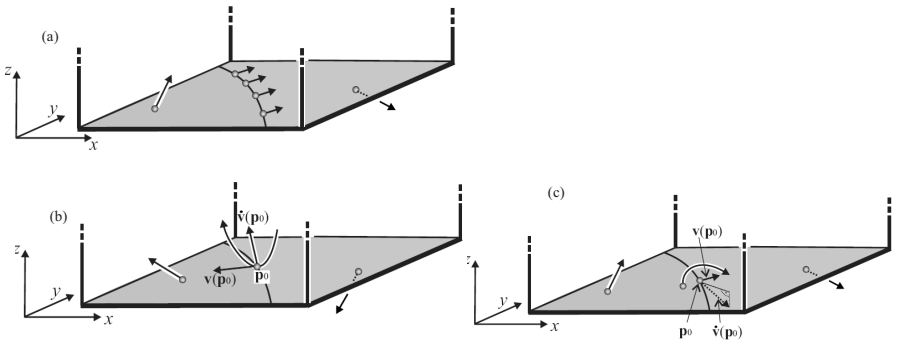

Fig. 9. (a) boundary plane $z = z_{min}$ consisting of an inflow area (blue), an outflow area (red), and their separating boundary switch curve; shown are 4 vectors of $\mathbf{v}$ on the boundary switch curve, and one each in the inflow and outflow area; (b) inbound point $\mathbf{p}_0$ on a boundary switch curve: $\mathbf{v}(\mathbf{p}_0)$ points into the inflow area, $\dot{\mathbf{v}}(\mathbf{p}_0)$ points inside D; shown is a part of the stream line starting in $\mathbf{p}_0$ both in forward and backward integration; (c) outbound point $\mathbf{p}_0$ on a boundary switch curve; $\mathbf{v}(\mathbf{p}_0)$ points into the outflow area, $\dot{\mathbf{v}}(\mathbf{p}_0)$ points outside D; shown is a stream line close to $\mathbf{p}_0$ starting in the inflow area and leaving D in the outflow area.

$z = z_{min}$ consisting of one inflow and one outflow area. (In the following we illustrate the concept of boundary switch curves only on the boundary plane $z = z_{min}$. Similar statements hold for the 5 remaining boundary planes of D.)

Given a point $\mathbf{p}_0$ on a boundary switch curve, two cases are possible concerning the stream line starting at $\mathbf{p}_0$:

- Starting from $\mathbf{p}_0$, the stream line integration moves inside D for both backward and forward integration. We call this point an *inbound point* on the boundary switch curve (Figure 9(b)).
- Starting from $\mathbf{p}_0$, the stream line integration moves outside D for both backward and forward integration. Therefore, this stream line in D consists only of $\mathbf{p}_0$ itself. We call this point an *outbound point* (Figure 9(c)).

Separatrices

Separatrices are curves or surfaces which separate regions of different flow behavior. Since around sources and sinks a homogeneous flow behavior is present (either a complete outflow or inflow), sources and sinks do not contribute to separatrices. A repelling saddle $\mathbf{x}_R$ creates two separatrices: one separation curve (which is a stream line starting in $\mathbf{x}_R$ in the inflow direction by backward integration) and a separation surface (which is a stream surface starting in the outflow plane by forward integration). Separatrices are also emanating from inbound segments of boundary switch curves.

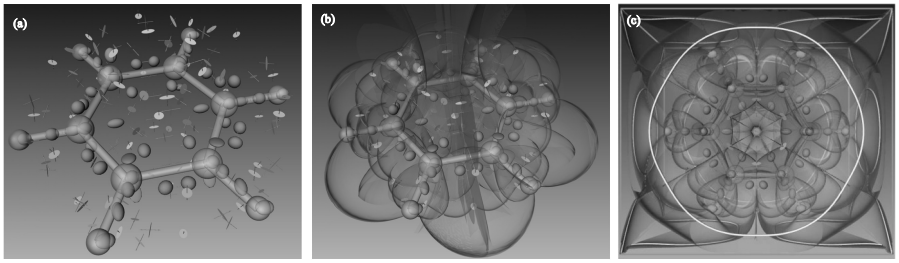

Fig. 10. Topological representations of the benzene data set with 184 critical points; (a) iconic representation; (b) separation surfaces starting from saddles; (c) separation surfaces starting from saddles and boundary switch curves (from [36, 43]).

Figure 10 shows the topological visualization of a data set describing the electrostatic field of a Benzene molecule[7]. Figure 10(a) shows the iconic representation of all 184 critical points. Figure 10(b) shows the critical points and the separation surfaces starting from the saddles, while figure 10(c) additionally shows the separatrices emanating from boundary switch curves.

Saddle- and boundary switch connectors

A saddle connector is the intersection curve between a separation surface starting from an attracting saddle and a separation surface starting from a repelling saddle. Figure 11(a),(b) give an illustration.

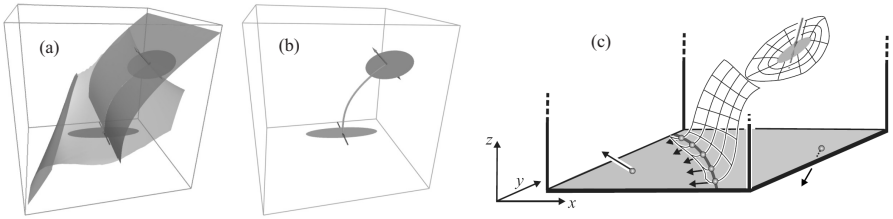

Fig. 11. (a) separation surfaces of two saddles; (b) the intersection of the separation surfaces is the saddle connector; (c) finding the intersection of two separation surfaces one comes from a saddle, while the other one comes from a boundary switch curve (from [36, 43]).

Boundary switch connectors are the intersection curves of separation surfaces starting from saddles or boundary switch curves. Figure 11(c) illustrates this. Concerning the different kinds of separation surfaces, 4 kinds of boundary switch connectors are possible. They are shown in figure 12

[7] This data set was calculated on a 101^3 regular grid using the fractional charges method described in [28].

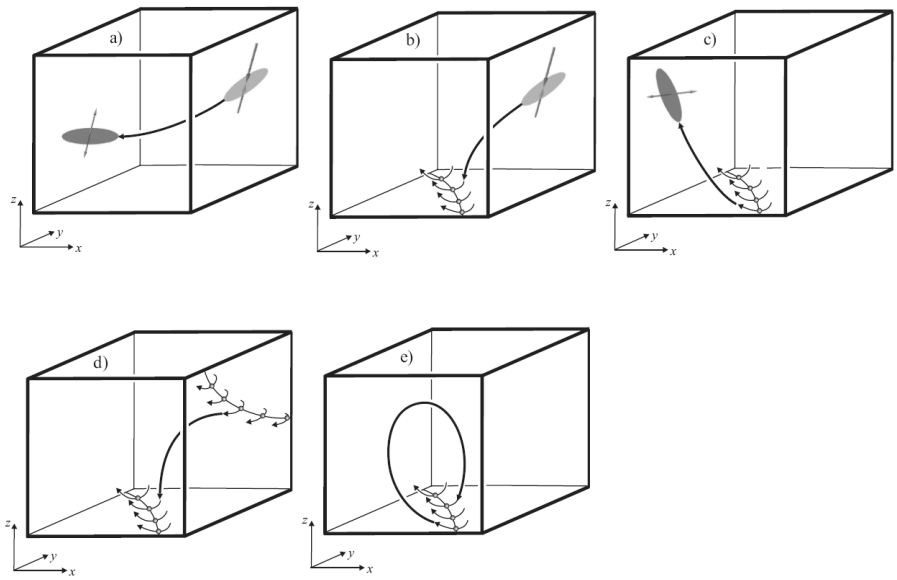

Fig. 12. Cases of intersection curves of separation surfaces: a) saddle connectors; b)-e) boundary switch connectors (from [43]).

3.2 Visualizing 3D topology

Given a 3D vector field $\mathbf{v}$, the critical points can be extracted directly (if $\mathbf{v}$ is piecewise linear) or numerically. Then the classification is done by an eigenvalue/eigenvector analysis of the Jacobian matrix.

Stream surfaces are obtained by a numerical stream surface integration [15, 25]. A standard approach is a 4th order Runge-Kutta integration. The result is a triangular mesh representing the stream surface which can be represented in a semitransparent way (figures 10(b),(c)).

Saddle connectors can serve as a visual alternative to visualizing separation surfaces since they tend to hide themselves and other features and thus produce cluttered visual representations (figures 10(b),(c)). In order to extract saddle connectors, stream surfaces have to be intersected. To do so, the front of the evolving stream surfaces are observed for intersection. Figure 13 gives an illustration. Boundary switch connectors are extracted in a similar way.

Example:

Figures 14a–d visualize a snapshot of a transitional wake behind a circular cylinder [48]. This flow exhibits periodic vortex shedding leading to the well known von Kármán vortex street. This phenomenon plays an important role in many industrial applications, like mixing in heat exchangers or mass flow measurements with vortex counters. However, this vortex shedding can lead

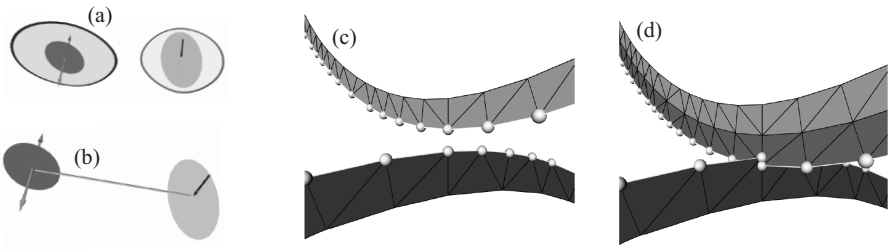

Fig. 13. Extracting a saddle connector: (a) simultaneously observe fronts of evolving stream surfaces; (b) stream line integration from intersection point gives saddle connector; (c) closeup shortly before intersection is found; (d) intersection is found (from [36]).

to undesirable periodic forces on obstacles, like chimneys, buildings, bridges and submarine towers.

This data set was derived from a direct numerical simulation of the Navier-Stokes equation by Gerd Mutschke [20]. The data resolves the so-called 'mode A' of the 3D transition at a Reynolds number of 200 and at a spanwise wavelength of 4 diameters. The figures display a small near-wake region of a large computational domain. All 13 critical points are contained in the shown domain and on its boundaries 13 boundary switch curves are observed. Together they span the topological skeleton of the incompressible velocity field.

The inspection of figure 14a suggests a high amount of circulating flow behavior in the data set, but due to the occlusion effects introduced by the separation surfaces neither the flow behavior on the boundaries nor the critical points can be seen easily. This complicates further examinations to a high degree.

The simplified topological skeletons shown in Figures 14b–d enable to reduce this high-dimensional data set to a simple conceptual flow representation from which qualitative conclusions can be drawn. Using connectors, the skeleton elucidates the symmetry of the mode A with respect to a plane which is perpendicular to the cylinder axis. The high number of spanwise and transverse running connectors of a single snapshot already indicate the experimentally observed good mixing properties of vortex shedding.

4 Topological features of time-dependent vector fields

Up to now we treated the topology of steady (time-independent) vector fields by segmenting areas of similar behavior of the stream lines. For time-dependent vector fields, there are two important classes of characteristic curves: stream lines and path lines. Hence, two different kinds of topologies can be obtained: a stream line and a path line oriented topology. We explain both concepts for 2D time-dependent vector fields and mention that – except

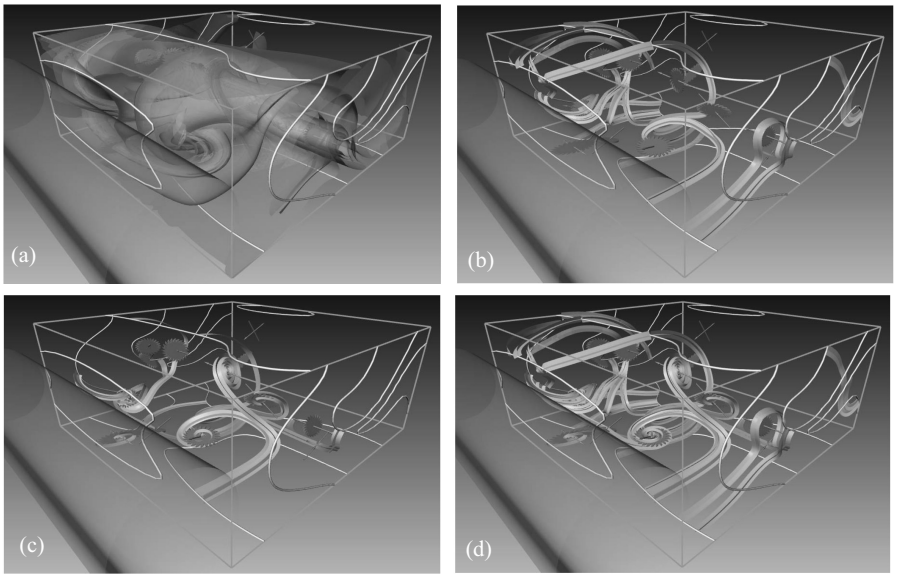

Fig. 14. Flow behind a circular cylinder: (a) separation surfaces emanating from boundary switch curves and saddles; (b) boundary switch connectors between boundary switch curves; (c) boundary switch connectors between saddle points and boundary switch curves; (d) saddle connectors and both types of boundary switch connectors (from [43]).

for some special configurations [8] – the topology of 3D time-dependent vector field is rather unsolved.

Given a 2D time-dependent vector field

$$\mathbf{v}(x,y,t) = \begin{pmatrix} u(x,y,t) \\ v(x,y,t) \end{pmatrix}, \tag{8}$$

where (x,y) describe the 2D domain and t is the temporal component, stream and path lines are generally different classes of curves. Stream lines are the tangent curves of $\mathbf{v}$ for a fixed time t, while path lines describe the paths of massless particles in $\mathbf{v}$ over time. To capture both types of lines, we define two 3D vector fields and consider their topological behavior.

To treat stream lines and path lines of $\mathbf{v}$, we consider

$$\mathbf{s}(x,y,t) = \begin{pmatrix} u(x,y,t) \\ v(x,y,t) \\ 0 \end{pmatrix} \quad , \quad \mathbf{p}(x,y,t) = \begin{pmatrix} u(x,y,t) \\ v(x,y,t) \\ 1 \end{pmatrix}. \tag{9}$$

Both $\mathbf{s}$ and $\mathbf{p}$ can be seen as a steady 3D vector field. The stream lines of $\mathbf{s}$ coincide with the stream lines of $\mathbf{v}$, since any integration step in $\mathbf{s}$ keeps the time component unchanged. Any (x,y)-slice through $\mathbf{s}$ represents $\mathbf{v}$ at a

constant time. The stream lines of $\mathbf{p}$ coincide with the path lines of $\mathbf{v}$: given a starting point $(\mathbf{x}_0, t_0)$, one step of a simple Euler approximation of $\mathbf{p}$ would be

$$\begin{pmatrix} \mathbf{x}_1 \\ t_1 \end{pmatrix} = \begin{pmatrix} \mathbf{x}_0 \\ t_0 \end{pmatrix} + d\ \mathbf{p}(\mathbf{x}_0, t_0) = \begin{pmatrix} \mathbf{x}_0 + d\ \mathbf{v}(\mathbf{x}_0, t_0) \\ t_0 + d \end{pmatrix} \tag{10}$$

which does not only change the location but also goes forward in time.[8] Figure 15 illustrates $\mathbf{s}$ and $\mathbf{p}$ for a simple example vector field $\mathbf{v}$. Note that in all

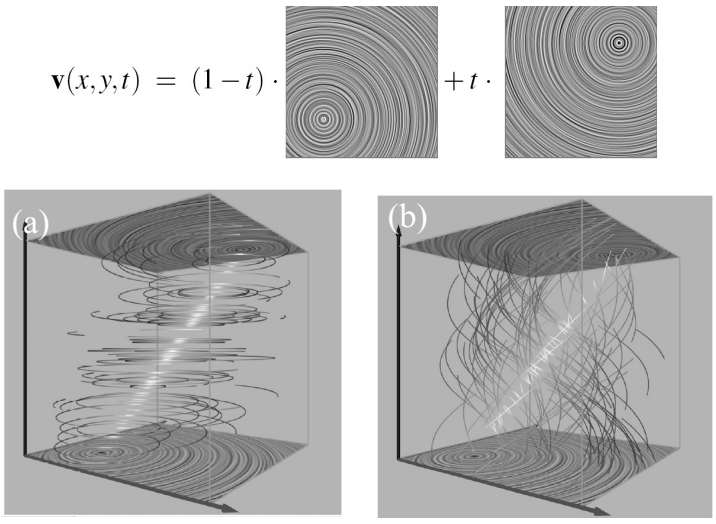

Fig. 15. Characteristic curves of a simple 2D time-dependent vector field shown as illuminated field lines: Stream lines of $\mathbf{s}$ correspond to the stream lines in $\mathbf{v}$; (b) stream lines of $\mathbf{p}$ correspond to the path lines in $\mathbf{v}$.

figures throughout this section the coordinate system is shown as follows: red/green coordinate axes denote the (x, y)-domain, the blue axis shows the time component.

Now the problem of finding a stream line and path line oriented topology is simply reduced to finding the topological skeletons of $\mathbf{s}$ and $\mathbf{p}$ respectively. Unfortunately, neither for $\mathbf{s}$ nor for $\mathbf{p}$ the classical vector field topology extraction techniques for 3D vector fields are applicable: $\mathbf{s}$ consists of critical lines while $\mathbf{p}$ does not have any critical points at all.

4.1 Stream line oriented topology

Stream line oriented topology is well-understood in the visualization community ([14], [1], [3]). In addition to track the topological features over time,

[8] For the actual integration one may use a fourth-order Runge-Kutta method.

bifurcations have to be extracted. Bifurcations are the events of structural changes of the flow behavior at a certain time. We can distinguish between local and global bifurcations depending on whether a local or a global analysis is necessary to extract them.

Tracking critical points

Critical points are important topological features of steady vector fields. Tracking their location over time is necessary for capturing the topological behavior of $\mathbf{v}$. This is equivalent to extracting the zero lines of $\mathbf{s}$, where all points on these lines are zero points of $\mathbf{v}$ at a certain time. To do so, one can either extract and connect the zeros on the faces of an underlying prism cell grid ([41]), or a feature flow field integration from a start zero point of $\mathbf{s}$ is applied. The feature flow field for tracking critical points is a 3D vector field $\mathbf{f}$ which points into the direction where all components of $\mathbf{s}$ remain unchanged. [34] shows that

$$\mathbf{f}(x,y,t) = \begin{pmatrix} \det(\mathbf{v}_y, \mathbf{v}_t) \\ \det(\mathbf{v}_t, \mathbf{v}_x) \\ \det(\mathbf{v}_x, \mathbf{v}_y) \end{pmatrix}. \tag{11}$$

Starting a stream line integration of $\mathbf{f}$ from a point $\mathbf{x}_0$ with $\mathbf{s}(\mathbf{x}_0) = (0,0,0)^T$, all points $\mathbf{x}$ on this stream line fulfill $\mathbf{s}(\mathbf{x}) = (0,0,0)^T$ as well.

To extract all critical lines of $\mathbf{s}$, an appropriate number of starting points is needed. We get them by considering all critical points at the boundaries of the domain of $\mathbf{s}$ (which can easily be obtained as critical points of 2D vector fields) and by additionally considering all *fold bifurcations* of $\mathbf{v}$. A fold bifurcation appears if at a certain time t a critical point appears, and in the same moment splits up to a saddle and source/sink/center.[9] Fold bifurcations can be found as the zeros of the following system of equations: $[u = 0,\ v = 0,\ \det(\mathbf{v}_x, \mathbf{v}_y) = 0]$ which can be solved numerically.

Another important class of local bifurcations are *Hopf bifurcations* denoting locations where a sink becomes a source or vice versa. Thus, this denotes the location of a center, i.e. a critical point with a vanishing divergence and a positive Jacobian. Hopf bifurcations can be extracted similar to fold bifurcations by numerically solving the system $[u = 0,\ v = 0,\ \mathrm{div}(\mathbf{v}) = u_x + v_y = 0]$ for (x,y,t) and selecting all isolated solutions with positive Jacobian.

Another part of the topological skeleton of $\mathbf{v}$ are the separation curves starting from saddle points. It is a well-known fact that a saddle of a 2D vector field creates 4 separation curves by starting the integration into the directions of the eigenvectors of the Jacobian matrix. While the saddle moves over time in $\mathbf{v}$, their swept surfaces form 4 stream surfaces dividing $\mathbf{s}$ into areas of different flow behavior. Figure 16(a),(b) gives an illustration of a simple vector field containing all topological feature mentioned above. In this figure (as

[9] Or the other way around: a saddle and a source/sink/center collapse and disappear.

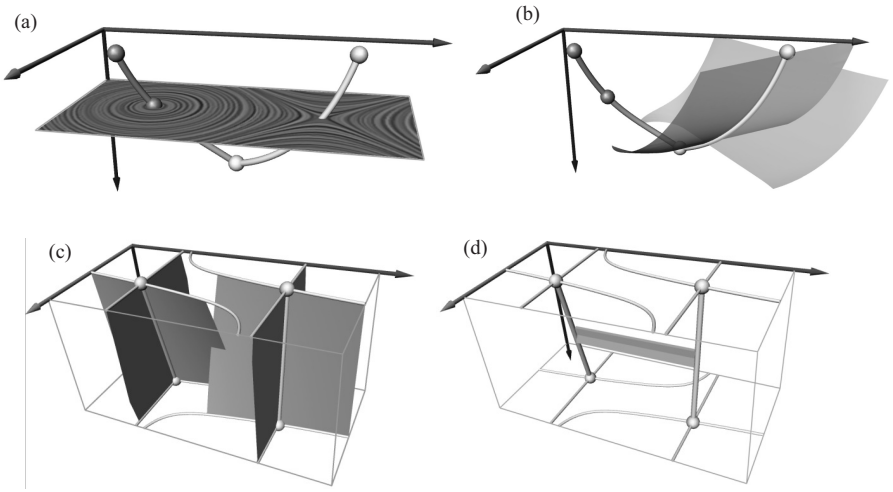

Fig. 16. (a),(b) topological visualization of a simple 2D time-dependent vector field consisting of sink, source, saddle, fold and Hopf bifurcation - one of each type: (a) critical lines of **s**, LIC plane through Hopf bifurcation; (b) separation surfaces created by the moving saddle. (c),(d) Extracting saddle connections: (c) separation surfaces starting from critical lines of **s**; (d) saddle connection as the intersection of these surfaces (from [38]).

well as in the following figures) we use the following color coding: the critical lines of **s** are color coded according to the inflow/outflow behavior of the represented critical points in **v**: a red/blue/green/yellow line segment represents a source/sink/center/saddle critical point respectively. The same color coding is used for particular critical points which are visualized as small spheres. This means that a Hopf bifurcation is shown as a small green sphere. Furthermore, fold bifurcations are shown as gray sphere, while particular stream lines of **s** are shown as gray lines. For integrated separation surfaces we color code according to the integration direction as red (forward integration) or blue (backward integration) surfaces.

Saddle connections

Saddle connections are global bifurcations which appear when two separatrices starting from saddle points collapse, i.e. when a separatrix of one saddle ends in another saddle. To extract them, we modify the idea of saddle connectors of 3D vector fields [36]: instead of starting the integration of one separation surface at each saddle of a 3D vector field, we start in the critical lines of **s** which represent a moving saddle. In fact, we start four stream surface integrations[10] at the critical lines of **s** into the directions of the eigenvectors of the

[10] Two forwards and two backwards.

Jacobian matrix. The rest of the algorithm is similar to saddle connectors [36] and yields all saddle connections in $\mathbf{v}$. Figure 16(c),(d) give an illustration.

A special case of saddle connections is the so-called *periodic blue sky bifurcation* ([1]) where two separatrices of the same saddle collapse. The algorithm described above to extract saddle connections automatically extracts these bifurcations as well. Figure 17 illustrates this.

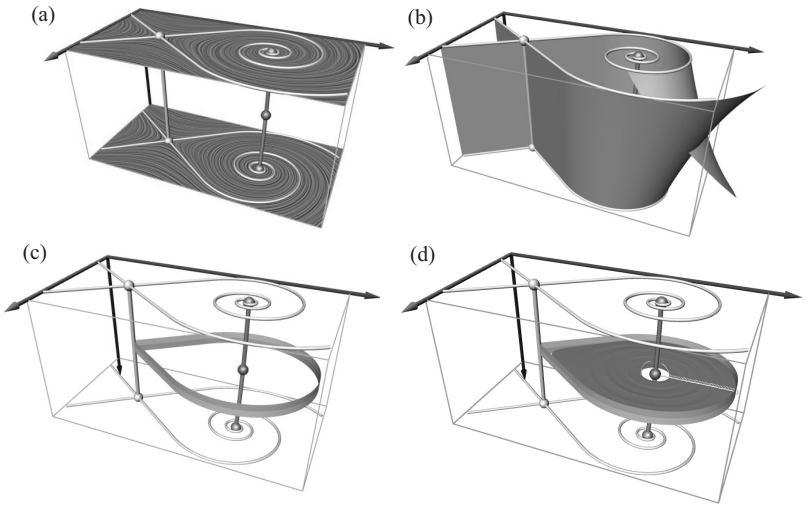

Fig. 17. Periodic blue sky bifurcation: (a) critical lines of s and two LIC planes; (b) separation surfaces shortly after their intersection; (c) two separation curves of the same saddle collapse; (d) tracked closed stream line starting from Hopf bifurcation. (from [38])

Tracking closed stream lines

Closed stream lines are global topological features which evolve over time in $\mathbf{v}$. Doing so, several bifurcations can occur: a closed stream line may appear or disappear, or two closed stream lines may collapse and disappear. The last case is called *cyclic fold bifurcation*.

To track isolated closed stream lines, an extraction in different time slices and subsequent linking was demonstrated in [47]. [38] presents a solution based on feature flow fields which works on space-time and can detect cyclic fold bifurcations as well. Figure 17(d) given an illustration.

4.2 Path line oriented topology

Considering a path line oriented topology for visualization purposes is a relatively new research area. Constructing a path line oriented topology means

to consider the stream lines of **p** and segment **p** into regions of different flow behavior of them. [38] introduces an approach which does the segmentation based on local path line properties. This way the domain segmented into areas where the path lines have attracting, repelling, or saddle like behavior.

4.3 An Example:

Figure 18 shows the visualization of a vector field describing the flow over a 2D cavity[11]. 1000 time steps have been simulated using the compressible Navier-Stokes equations; it exhibits a non-zero divergence inside the cavity, while outside the cavity the flow tends to have a quasi-divergence-free behavior. Figure 18 shows approximately one period, 100 time steps, of the full data set. Figures 18 both reveal the overall movement of the topological structures, the most dominating ones originating in or near the boundaries of the cavity itself. The quasi-divergence-free behavior outside the cavity is confirmed by the fact that a high number of Hopf bifurcations has been found in this area.

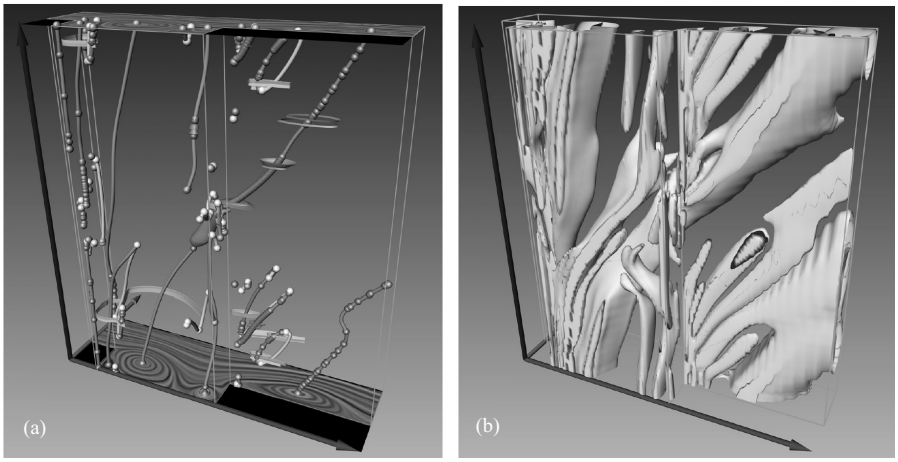

Fig. 18. 2D time-dependent flow at a cavity: (a) stream line oriented topology of the first 100 time steps; (b) path line oriented topology of the first 100 time steps (from [38]).

5 Further applications of topological features

Topological features of vector fields have not only proved to be a valuable visualization tool, they can also be used for other task in processing vector fields.

[11] This data set was kindly provided by Mo Samimy and Edgar Caraballo (both Ohio State University) [30] as well as Bernd R. Noack and Ivanka Pelivan (both TU Berlin).

Here we introduce approaches to compress, simplify, compare, and construct vector fields based on topological methods.

5.1 Compressing vector fields

Flow data sets (i.e., vector fields) tend to be large and complex. This fact has motivated an intensive research in simplifying and compressing vector fields. For both challenges, topological concepts have been applied. Compression techniques for vector fields are motivated by the necessity of transmitting large flow data sets over networks with low bandwidth, or by the goal to produce visualizations of the data in low-end machines with a small main memory. For these cases the consideration of compressed vector fields makes the process of visual analysis of the flow data more efficient and is sometimes the only way to process the data in reasonable time rates at all.

The main idea of a (lossy) data compression is to reduce the amount of data while keeping the important structures. Since generally the topological skeleton is known to give a compact description of the global flow behavior, topology preserving compression techniques are an obvious approach. Lodha et al. [18, 17] introduce a compression technique for 2D vector fields which prohibits strong changes of location and Jacobian matrix of the critical points.

Theisel et al. [32] introduce an approach which guarantees that the topology of original and compressed vector field coincides both for critical points and for the connectivity of the separatrices. It is shown that even under these strong conditions high compression ratios for vector fields with complex topologies are achieved. The method works on a piecewise linear vector field over a triangulation. The vector field is interpreted as a piecewise triangular mesh. Then a standard mesh reduction algorithm can be adapted to this specific problem, i.e. the compression is achieved by iteratively applying half-edge collapses. Before a half-edge collapse is carried out, it is checked that it does not change the global topology of the vector field. As the theoretical foundation of the algorithm in [32], it is shown that for local modifications of a vector field, it is possible to decide entirely by a local analysis whether or not the global topology is preserved.

Figure 19 shows the application of the compression algorithm to a data set of a complex topology. Figure 19(a) shows the underlying triangular grid of the data set consisting of 12,726 triangles. Figure 19(c) shows the topological skeleton consisting of 338 critical points, 34 boundary switch points, and 714 separatrices. Figure 19(b) shows the underlying triangular grid after applying the compression algorithm. This grid contains of 2,153 triangles. The topological skeleton of the compressed vector field is shown in figure 19(d).

5.2 Topological simplification of vector fields

The topological skeleton of a vector field may be very complex due to the presence of noise. In this case, unimportant topological features have to be

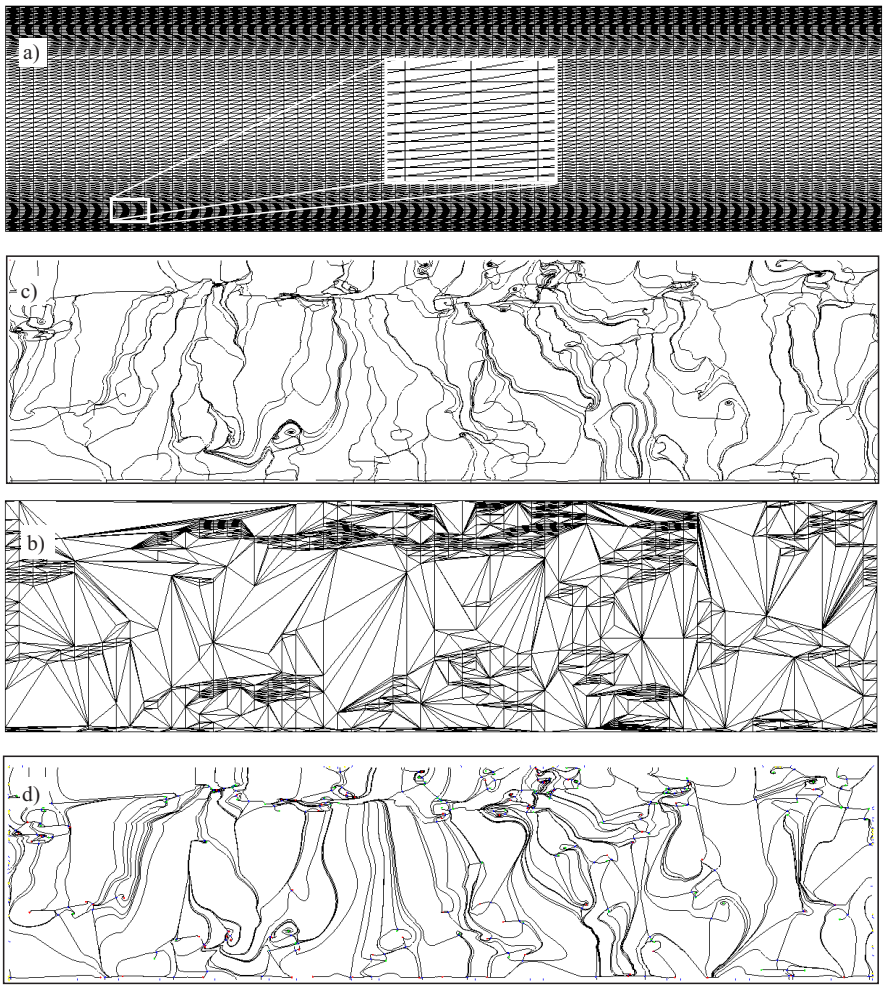

Fig. 19. (a) piecewise triangular domain of the original data set; (b) piecewise triangular domain of the compressed data set; (c) topological skeleton of original data set; (d) topological skeleton of compressed data set (from [32]).

removed. This is done by a topological simplification. The simplest way to do so is to apply a smoothing of the vector field before extracting the topology ([6]). More involved techniques start with the original topological skeleton and repeatedly apply local modifications of the skeleton and/or the underlying vector field in order to remove unimportant critical points. They are based on the index theorem for vector fields which ensures that the sum of the indices of the critical points remains constant in the modified area. (See [7] or another textbook on vector analysis for an introduction of the index of critical points and the index theorem.)

De Leeuw and van Liere [5] denote the importance of a critical point (source or sink) by computing the area from which the flow ends in forward or backward integration. Based on this area metric, the unimportant critical points are repeatedly collapsed to more important critical points in the neighborhood. [6] finds couples of first order critical points by considering distance and connectivity of them. Then the unimportant critical points are pairwise removed. Tricoche et al. [40] use a similar approach but provide a way of consistently updating the underlying vector field.

Theisel et al. [31] solve the coupling problem of critical points by a feature flow field approach. This gives not only the couples of critical points but also provides them and the separatrices with an importance weight. Then topological features with an importance below a certain threshold can be removed. Figure 20 gives an illustration.

Tricoche et al. [39] present another approach to simplifying the topology of 2D vector fields by replacing clusters of first order critical points with a higher order critical point. Weinkauf et al. [45] extend this to 3D vector fields. Figure 21 illustrates this.

5.3 Topological comparison of vector fields

To deal with the increasing size and complexity of the vector fields, a number of reconstruction, compression and simplification techniques have been introduced. All these techniques rely on certain distance measures between vector fields: the original and the derived vector field have to be compared to guarantee a sufficient similarity between them. Hence the definition of useful metrics on vector fields plays a crucial role in the applications above. The first approaches on metrics (distance measures) of vector fields consider local deviations of direction and magnitude of the flow vectors in a certain number of sample points ([12], [29]). These distance functions give a fast comparison of the vector field but do not take any structural information of the vector fields into consideration.

A first approach to define a topology based distance function was given in [16]. Given two vector fields $\mathbf{v}_1$ and $\mathbf{v}_2$, all critical points are extracted and coupled. Then the distance of the vector fields is obtained as sum of the distances of the corresponding critical points in $\mathbf{v}_1$ and $\mathbf{v}_2$. To compute the distance between two critical points, a number approaches exist [16, 35]. To couple the points, [33] proposes to use feature flow fields: a time-dependent vector field $\mathbf{v} = (1-t)\,\mathbf{v}_1 + t\,\mathbf{v}_2$ is constructed in which the critical points are tracked by a stream line integration of (11).

We demonstrate the application of topological comparison on a real data set. Figure 22(a) shows the visualization of a 2D flow in a bay area of the Baltic Sea near Greifswald, Germany (Greifswalder Bodden) at two different

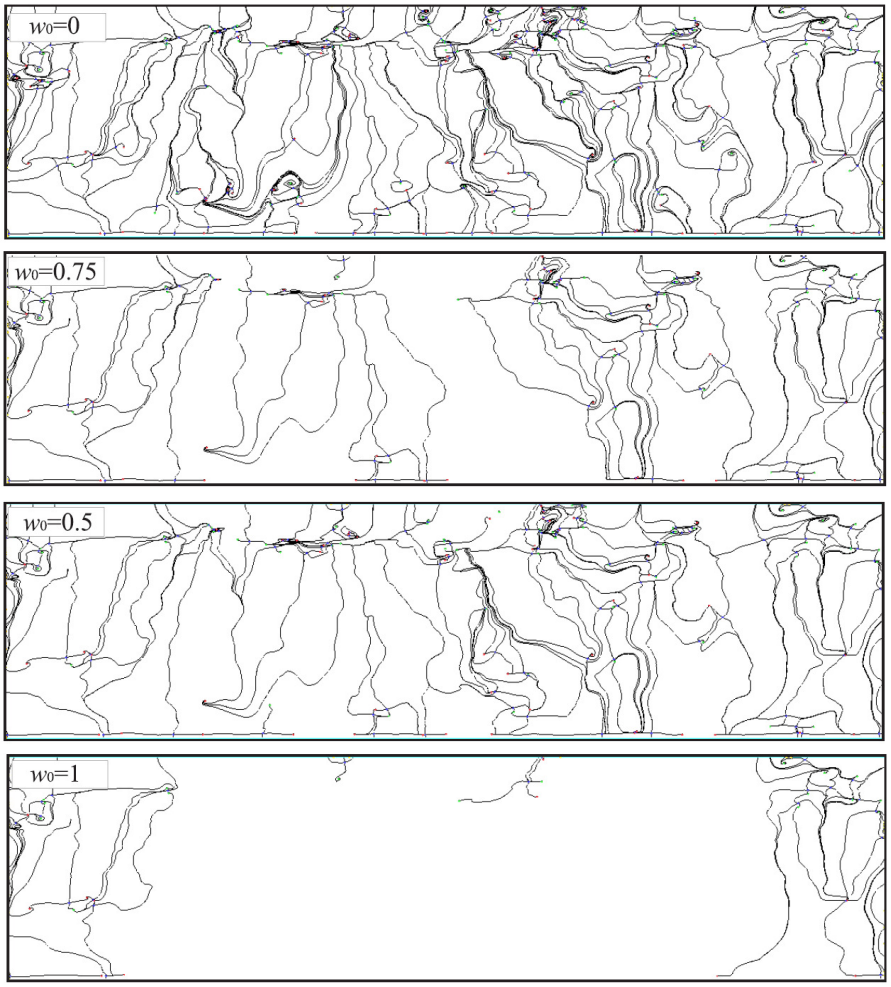

Fig. 20. Important topological features for different thresholds w_0; the image upper left ($w_0 = 0$) shows the complete topological skeleton. (from [31]).

time steps[12]. The data set can be considered as a collection of 25 vector fields $\mathbf{v}_0, ..., \mathbf{v}_{24}$. To evaluate the temporal behavior of the topology, the topological distance of each time step with all other time steps is computed. As an example, figure 22(a) illustrates the computation of the distance of the vector fields $\mathbf{v}_5$ and $\mathbf{v}_{10}$. Shown are the topological skeletons of $\mathbf{v}_5$ and $\mathbf{v}_{10}$ as well as the integration of the stream lines of the feature flow field starting in the

[12] This data set was obtained by a numerical simulation on a regular 115×103 grid at 25 time steps. It was created by the Department of Mathematics, University of Rostock (Germany).

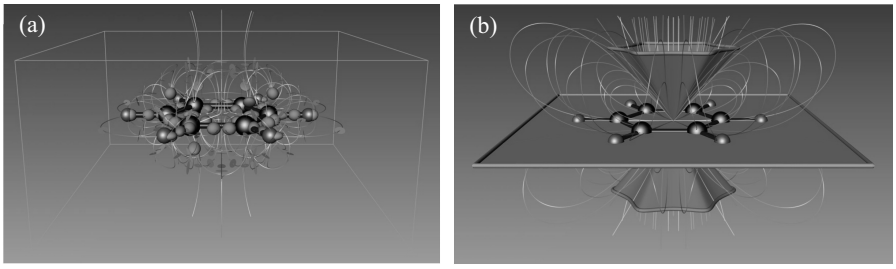

Fig. 21. Topological representations of the electrostatic field of the Benzene molecule: (a) 184 first order critical points. The box around the molecule represents the chosen area for topological simplification. (b) Topologically simplified representation with one higher order critical point elucidates the far field behavior of the benzene (from [45]).

critical point. We can see that most of the points find their partners in the other vector field. Figures 22(b),(c) show magnifications of figure 22(a). Figure 22(d) shows the color coded distance matrix of all vector fields $\mathbf{v}_0, ..., \mathbf{v}_{24}$. The distance varied between 0 and a maximal value of 104.5 (which was detected between $\mathbf{v}_3$ and $\mathbf{v}_{24}$). The distance was linearly color coded in such a way that a zero distance corresponds to black while the maximal distance corresponds to white. Figure 22(d) shows that the distance matrix is symmetric and with a zero main diagonal. The most important observation which can be made from figure 22(d) is that the distance of two vector fields $\mathbf{v}_i$ and $\mathbf{v}_j$ is approximately proportional to the distance $\|i-j\|$ of the time indices. This means that the rate of change of the topology is approximately linear over time. This result is particularly interesting if the number of critical points in the vector fields $\mathbf{v}_0, ..., \mathbf{v}_{24}$ is considered. They are (in this order) 65, 71, 71, 68, 65, 71, 63, 62, 66, 64, 65, 63, 70, 70, 51, 61, 52, 50, 56, 52, 63, 62, 72, 65. This shows that there is no correlation between the number of critical points and the topological distance: both $\mathbf{v}_0$ and $\mathbf{v}_{24}$ have the same number 65 of critical points but a maximal topological distance.

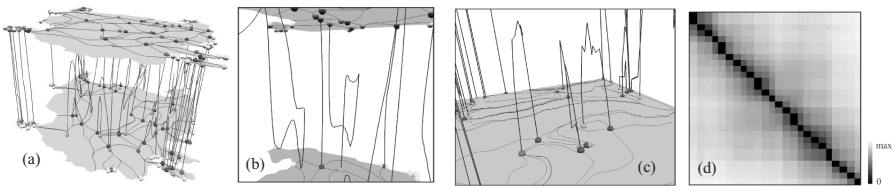

Fig. 22. (a) coupling the critical points of the $\mathbf{v}_5$ and $\mathbf{v}_{10}$ of the bay data set by integrating the stream lines of $\mathbf{f}$; (b),(c): magnifications of (a); (d) distance matrix between $\mathbf{v}_0, ..., \mathbf{v}_{24}$ (from [33]).

5.4 Constructing vector fields

The vector fields considered in flow visualization are usually obtained by a simulation or measurement process. Nevertheless they can also be obtained by construction. Applications of this approach are vector fields used for pattern matching, optimizing flow, education and testing new visualization techniques.

The approach of constructing vector fields is strongly related to the ideas of constructing curves and surfaces in the context of CAGD (Computer Aided Geometric Design). There the curves/surfaces are designed by creating a skeleton of control polygons (for instance Bezier- or B-spline polygons). This skeleton contains the relevant information of the curve/surface in an intuitive way. [30] presents an approach to transform the CAGD methods to the construction of 2D vector fields. To do so, first the topological skeleton of a vector field is constructed by a number of control polygons. As a second step, a piecewise linear vector field of exactly the specified topology is automatically created. Figure 23 gives an example.

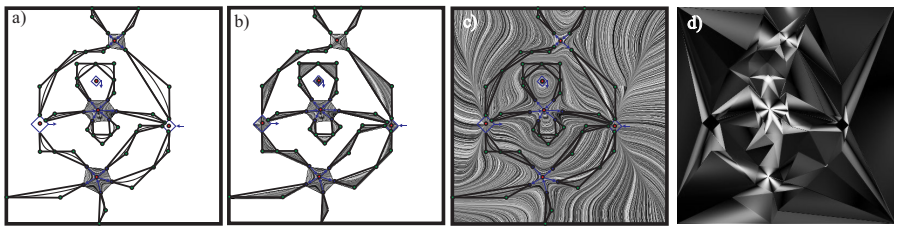

Fig. 23. Constructing a 2D vector field; a) topological skeleton of a vector field containing a number of higher order critical points; b) piecewise linear vector field describing the constructed topological features, i.e. the critical points and separatrices; c) complete piecewise linear vector field; d) curvature plot (from [30]).

An approach to constructing 3D vector fields is presented in [44]. There, the skeleton is modeled by interactively moving a number of control polygons determining location and characterization of the (first or higher order) critical points and the saddle connectors. Then a piecewise linear vector field is automatically constructed which has the same topological skeleton as modeled before. This approach is based on a complete segmentation of the areas around critical points into sectors of different flow behavior. Based on this, an approach to visualizing higher order critical points of 3D vector fields is presented.

Figure 24(a) shows a modeled topological skeleton consisting of 6 critical points and 8 connectors. Each of the critical points consists of two hyperbolic sectors and is actually a first order saddle point. Each of the connectors was defined by specifying start and end point and omitting any intermediate points. Thus, each connector consists of one cubic segment. Figure 24(b)

shows the result of the tetrahedrization of the critical points and the connectors. In this figure we can clearly see that each connector is constructed in one tetrahedron. Figure 24(c) shows the complete tetrahedrization of the piecewise linear vector field consisting of 256 tetrahedra. Figures 24(d) and 24(e) show different visualizations of the newly constructed vector field. Figure 24(d) shows a stream surface integration of the separation surfaces. They are color coded in red (outflow surface) and blue (inflow surface). Figure 24(e) shows the extraction of saddle connectors [36] revealing that they coincide with the modeled connectors of figure 24(a). In addition, figure 24(e) shows a number of illuminated stream lines [49].

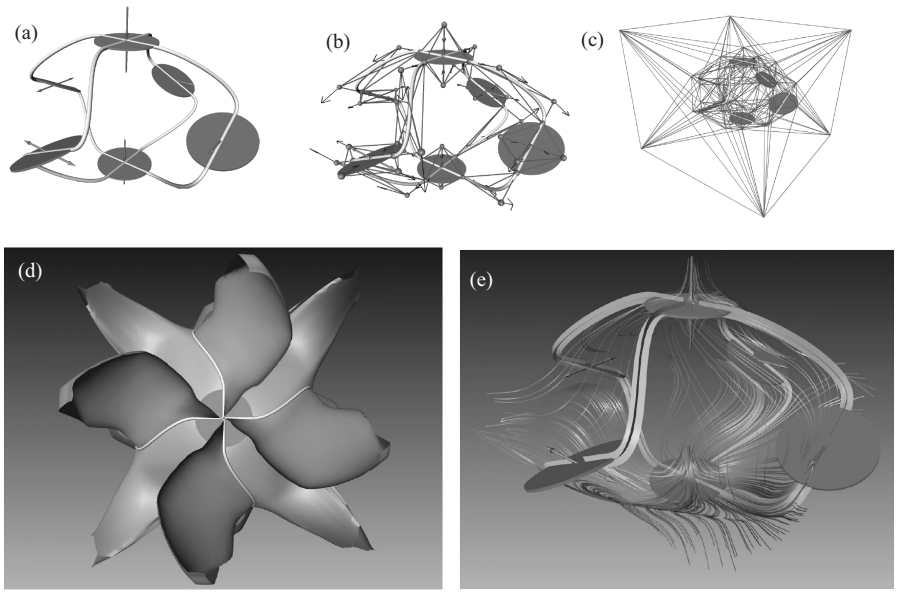

Fig. 24. Constructed 3D vector field: (a) Modeled topological skeleton; (b) Tetrahedrization of critical points and connectors; (c) Complete tetrahedrization; (d) Separation surfaces of constructed vector field, view from top; (e) Saddle connectors and stream lines of constructed vector field (from [44]).

6 Conclusions

In this chapter we have shown that topological methods provide a useful framework for the visual analysis of vector fields. However, there is a number of open problems which are still rather unsolved. Firstly, an appropriate visual representation of the topological skeleton of 3D time-dependent vector fields is still a challenge. Secondly, the path line oriented topological representation

of time-dependent vector fields remains an open problems. Because of this we expect an active ongoing research in the field in the next years.

References

1. L. Abraham and K. Shaw. *Dynamics, The Geometry of Behaviour*. Addison-Wesley, 1992.
2. D. Asimov. Notes on the topology of vector fields and flows. Technical report, NASA Ames Research Center, 1993. RNR-93-003.
3. P. G. Bakker. *Bifurcations in Flow Patterns (Theory and Applications of Transport in Porous Media)*. Kluwer Academic Publishers, 1991.
4. M. S. Chong, A. E. Perry, and B. J. Cantwell. A general classification of three-dimensional flow fields. *Physics of Fluids A*, 2(5):765–777, 1990.
5. W. de Leeuw and R. van Liere. Collapsing flow topology using area metrics. In *Proc. IEEE Visualization '99*, pages 149–354, 1999.
6. W. de Leeuw and R. van Liere. Visualization of global flow structures using multiple levels of topology. In *Data Visualization 1999. Proc. VisSym 99*, pages 45–52, 1999.
7. P.A. Firby and C.F. Gardiner. *Surface Topology*, chapter 7, pages 115–135. Ellis Horwood Ltd., 1982. Vector Fields on Surfaces.
8. C. Garth, X. Tricoche, and G. Scheuermann. Tracking of vector field singularities in unstructured 3D time-dependent datasets. In *Proc. IEEE Visualization 2004*, pages 329–336, 2004.
9. A. Globus, C. Levit, and T. Lasinski. A tool for visualizing the topology of three-dimensional vector fields. In *Proc. IEEE Visualization '91*, pages 33–40, 1991.
10. J. Guckenheimer and P. Holmes. *Nonlinear Oscillations, Dynamical Systems, and Bifurcations of Vector Fields*. Springer, 2nd edition, 1986.
11. H. Hauser and E. Gröller. Thorough insights by enhanced visualization of flow topology. In *9th international symposium on flow visualization*, 2000.
12. B. Heckel, G.H. Weber, B. Hamann, and K.I.Joy. Construction of vector field hierarchies. In D. Ebert, M. Gross, and B. Hamann, editors, *Proc. IEEE Visualization '99*, pages 19–26, Los Alamitos, 1999.
13. J. Helman and L. Hesselink. Representation and display of vector field topology in fluid flow data sets. *IEEE Computer*, 22(8):27–36, 1989.
14. J. Helman and L. Hesselink. Visualizing vector field topology in fluid flows. *IEEE Computer Graphics and Applications*, 11:36–46, May 1991.
15. J. Hultquist. Constructing stream surfaces in steady 3D vector fields. In *Proc. IEEE Visualization '92*, pages 171–177, 1992.
16. Y. Lavin, R.K. Batra, and L. Hesselink. Feature comparisons of vector fields using earth mover's distance. In *Proc. IEEE Visualization '98*, pages 103–109, 1998.
17. S. Lodha, N. Faaland, and J. Renteria. Topology preserving top-down compression of 2d vector fields using bintree and triangular quadtrees. *IEEE Transactions on Visualization and Computer Graphics*, 9(4):433–442, 2003.
18. S.K. Lodha, J.C. Renteria, and K.M. Roskin. Topology preserving compression of 2D vector fields. In *Proc. IEEE Visualization 2000*, pages 343–350, 2000.

19. H. Löffelmann, H. Doleisch, and E. Gröller. Visualizing dynamical systems near critical points. In *Spring Conference on Computer Graphics and its Applications*, pages 175–184, Budmerice, Slovakia, 1998.
20. G. Mutschke, 2003. private communication.
21. G.M. Nielson. Tools for computing tangent curves and topological graphs for visualizing piecewise linearly varying vector fields over triangulated domains. In G.M. Nielson, H. Hagen, and H. Müller, editors, *Scientific Visualization*, pages 527–562. IEEE Computer Society, 1997.
22. P. A. Philippou and R. N. Strickland. Vector field analysis and synthesis using three dimensional phase portraits. *Graphical Models and Image Processing*, 59:446–462, November 1997.
23. K. Polthier and E. Preuss. Identifying vector fields singularities using a discrete hodge decomposition. In H.-C. Hege and K. Polthier, editors, *Visualization and Mathematics III*, pages 135–150. Springer Verlag, Heidelberg, 2002.
24. F.H. Post, B. Vrolijk, H. Hauser, R.S. Laramee, and H. Doleisch. Feature extraction and visualisation of flow fields. In *Proc. Eurographics 2002, State of the Art Reports*, pages 69–100, 2002.
25. G. Scheuermann, T. Bobach, H. Hagen K. Mahrous, B. Hamann, K. Joy, and W. Kollmann. A tetrahedra-based stream surface algorithm. In *Proc. IEEE Visualization 01*, pages 151 – 158, 2001.
26. G. Scheuermann, H. Krüger, M. Menzel, and A. Rockwood. Visualizing nonlinear vector field topology. *IEEE Transactions on Visualization and Computer Graphics*, 4(2):109–116, 1998.
27. H. Schumann and W. Müller. *Visualisierung - Grundlagen und allgemeine Methoden*. Springer-Verlag, 2000. (in German).
28. D. Stalling and T. Steinke. Visualization of vector fields in quantum chemistry. Technical report, ZIB Preprint SC-96-01, 1996. ftp://ftp.zib.de/pub/zib-publications/reports/SC-96-01.ps.
29. A. Telea and J.J. van Wijk. Simplified representation of vector fields. In D. Ebert, M. Gross, and B. Hamann, editors, *Proc. IEEE Visualization '99*, pages 35–42, Los Alamitos, 1999.
30. H. Theisel. Designing 2D vector fields of arbitrary topology. *Computer Graphics Forum (Eurographics 2002)*, 21(3):595–604, 2002.
31. H. Theisel, Ch. Rössl, and H.-P. Seidel. Combining topological simplification and topology preserving compression for 2d vector fields. In *Proc. Pacific Graphics*, pages 419 – 423, 2003.
32. H. Theisel, Ch. Rössl, and H.-P. Seidel. Compression of 2D vector fields under guaranteed topology preservation. *Computer Graphics Forum (Eurographics 2003)*, 22(3):333–342, 2003.
33. H. Theisel, Ch. Rössl, and H.-P. Seidel. Using feature flow fields for topological comparison of vector fields. In *Proc. Vision, Modeling and Visualization 2003*, pages 521 – 528, Berlin, 2003. Aka.
34. H. Theisel and H.-P. Seidel. Feature flow fields. In *Data Visualization 2003. Proc. VisSym 03*, pages 141–148, 2003.
35. H. Theisel and T. Weinkauf. Vector field metrics based on distance measures of first order critical points. In *Journal of WSCG*, volume 10:3, pages 121–128, 2002.
36. H. Theisel, T. Weinkauf, H.-C. Hege, and H.-P. Seidel. Saddle connectors - an approach to visualizing the topological skeleton of complex 3D vector fields. In *Proc. IEEE Visualization 2003*, pages 225–232, 2003.

37. H. Theisel, T. Weinkauf, H.-C. Hege, and H.-P. Seidel. Grid-independent detection of closed stream lines in 2D vector fields. In *Proc. Vision, Modeling and Visualization 2004*, 2004.
38. H. Theisel, T. Weinkauf, H.-C. Hege, and H.-P. Seidel. Stream line and path line oriented topology for 2D time-dependent vector fields. In *Proc. IEEE Visualization 2004*, pages 321–328, 2004.
39. X. Tricoche, G. Scheuermann, and H. Hagen. A topology simplification method for 2D vector fields. In *Proc. IEEE Visualization 2000*, pages 359–366, 2000.
40. X. Tricoche, G. Scheuermann, and H. Hagen. Continuous topology simplification of planar vector fields. In *Proc. Visualization 01*, pages 159 – 166, 2001.
41. X. Tricoche, G. Scheuermann, and H. Hagen. Topology-based visualization of time-dependent 2D vector fields. In *Data Visualization 2001. Proc. VisSym 01*, pages 117–126, 2001.
42. T. Weinkauf. Krümmungsvisualisierung für 3D-Vektorfelder. Diplomarbeit, University of Rostock, Computer Science Department, 2000. (in German).
43. T. Weinkauf, H. Theisel, H.-C. Hege, and H.-P. Seidel. Boundary switch connectors for topological visualization of complex 3D vector fields. In *Proc. VisSym 04*, pages 183–192, 2004.
44. T. Weinkauf, H. Theisel, H.-C. Hege, and H.-P. Seidel. Topological construction and visualization of higher order 3D vector fields. *Computer Graphics Forum (Eurographics 2004)*, 23(3):469–478, 2004.
45. T. Weinkauf, H. Theisel, K. Shi, H.-C. Hege, and H.-P. Seidel. Extracting higher order critical points and topological simplification of 3D vector fields. In *Proc. IEEE Visualization 2005*, 2005.
46. T. Wischgoll and G. Scheuermann. Detection and visualization of closed streamlines in planar flows. *IEEE Transactions on Visualization and Computer Graphics*, 7(2):165–172, 2001.
47. T. Wischgoll, G. Scheuermann, and H. Hagen. Tracking closed stream lines in time-dependent planar flows. In *Proc. Vision, Modeling and Visualization 2001*, pages 447–454, 2001.
48. H.-Q. Zhang, U. Fey, B.R. Noack, M. König, and H. Eckelmann. On the transition of the cylinder wake. *Phys. Fluids*, 7(4):779–795, 1995.
49. M. Zöckler, D. Stalling, and H.C. Hege. Interactive visualization of 3D-vector fields using illuminated stream lines. In *Proc. IEEE Visualization '96*, pages 107–113, 1996.